

22 Radiation Damage Effects

R.-Y. Zhu

Physics, Mathematics and Astronomy Division, California Institute of
Technology, Pasadena, CA, USA

1	<i>Introduction</i>	536
2	<i>Scintillation-Mechanism Damage</i>	538
3	<i>Radiation-Induced Phosphorescence and Energy-Equivalent Readout Noise</i>	539
4	<i>Radiation-Induced Absorption</i>	539
4.1	Recovery of Radiation-Induced Absorption	542
4.2	Radiation-Induced Color Centers	543
4.3	Dose-Rate Dependence and Color-Center Kinetics	546
5	<i>Light-Output Degradation</i>	546
6	<i>Light-Response Uniformity</i>	547
7	<i>Damage Mechanism in Alkali Halide Crystals and CsI(Tl) Development</i>	549
8	<i>Damage Mechanism in Oxide Crystals and PWO Development</i>	551
9	<i>Conclusion</i>	553
	<i>Acknowledgments</i>	554
	<i>References</i>	554
	<i>Further Reading</i>	555

Abstract: Radiation damage is an important issue for the particle detectors operated in a hostile environment where radiations from various sources are expected. This is particularly important for high energy physics detectors designed for the energy and intensity frontiers. This chapter describes the radiation damage effects in scintillating crystals, including the scintillation-mechanism damage, the radiation-induced phosphorescence, and the radiation-induced absorption. The radiation damage mechanism in crystal scintillators is also discussed. While the damage in halides is attributed to the oxygen/hydroxyl contamination, it is the structure defects, such as the oxygen vacancies, which cause the damage in oxides. Various material analysis methods used in investigations of the radiation damage effects as well as the improvement of crystal quality through systematic R&D are also presented.

1 Introduction

Total-absorption shower counters made of inorganic crystal scintillators have been known for decades for their superb energy resolutions and detection efficiencies (Gratta et al. 1994). In high energy and nuclear physics experiments, large arrays of scintillating crystals of up to 10 m^3 have been assembled for precision measurement of photons and electrons. These crystals are working in a radiation environment, where various particles, such as γ rays, neutrons, and charged hadrons, are expected. **Table 1** (Mao et al. 2008) lists the basic properties of the heavy-crystal scintillators commonly used in high energy physics detectors. They are NaI(Tl), CsI(Tl), undoped CsI, BaF₂, bismuth germanate (BGO), lead tungstate (PWO), and Ce-doped lutetium oxyorthosilicate ($\text{Lu}_2(\text{SiO}_4)\text{O}$ or LSO(Ce)) (Melcher and Schweitzer 1992). All have either been used in, or actively pursued for, high energy and nuclear physics experiments. Some of them, such as NaI(Tl), CsI(Tl), BGO, LSO(Ce), and cerium-doped lutetium–yttrium oxyorthosilicate ($\text{Lu}_{2(1-x)}\text{Y}_{2x}\text{SiO}_5\text{:Ce}$, LYSO) (Cooke et al. 2000; Kimble et al. 2002) are also widely used in the medical industry.

All known crystal scintillators suffer from radiation damage (Zhu 1998). There are three possible radiation damage effects in crystal scintillators: (1) the scintillation-mechanism damage, (2) the radiation-induced phosphorescence (afterglow), and (3) the radiation-induced absorption (color centers). A damaged scintillation mechanism would reduce the scintillation light yield and cause a degradation of the light output. It may also change the light-response uniformity along the crystal length since the radiation dose profile is usually not uniform. The radiation-induced phosphorescence, commonly called afterglow, causes an increase of the dark current in the photodetectors, and thus an increase of the readout noise. The radiation-induced absorption reduces the light attenuation length (Ma and Zhu 1993), and thus the light output and possibly also the light-response uniformity.

Table 2 summarizes γ -ray-induced radiation damage effect for various crystal scintillators. There is no experimental data supporting a scintillation-mechanism damage. All crystal scintillators studies so far, however, suffer from the radiation-induced phosphorescence and the radiation-induced absorption.

The radiation-induced absorption is caused by a process called color-center formation, which may recover spontaneously under the application temperature through a process called color-center annihilation. If so, the damage would be dose-rate dependent (Ma and Zhu 1993, 1995; Zhu 1997). If the radiation-induced absorption does not recover, or the recovery speed is

■ **Table 1**
Properties of some heavy-crystal scintillators

Crystal	NaI(Tl)	CsI(Tl)	CsI	BaF ₂	BGO	PWO	LSO(Ce)
Density (g/cm ³)	3.67	4.51	4.51	4.89	7.13	8.3	7.40
Melting point (°C)	651	621	621	1280	1050	1123	2050
Radiation length (cm)	2.59	1.86	1.86	2.03	1.12	0.89	1.14
Molière radius (cm)	4.13	3.57	3.57	3.10	2.23	2.00	2.07
Interaction length (cm)	42.9	39.3	39.3	30.7	22.7	20.7	20.9
Refractive index ^a	1.85	1.79	1.95	1.50	2.15	2.20	1.82
Hygroscopicity	Yes	Slight	Slight	No	No	No	No
Luminescence ^b (nm) (at Peak)	410	560	420	300	480	425	420
			310	220		420	
Decay time ^b (ns)	245	1220	30	650	300	30	40
			6	0.9		10	
Light yield ^{b,c}	100	165	3.6	36	21	0.30	85
			1.1	4.1		0.077	
d(LY)/dT ^{b,d} (%/°C)	-0.2	0.4	-1.4	-1.9	-0.9	-2.5	-0.2
				0.1			
Experiment	Crystal	CLEO	KTeV	TAPS	L3	CMS	KLOE
	Ball	BaBar			BELLE	ALICE	SuperB
		BELLE				PrimEx	
		BES III				Panda	

^aAt the wavelength of the emission maximum

^bTop line: slow component, bottom line: fast component

^cRelative light yield of samples of 1.5 X₀ and with the PMT QE taken out

^dAt room temperature

■ **Table 2**
Radiation damage in crystal scintillators

Item	CsI(Tl)	CsI	BaF ₂	BGO	PWO	LSO/LYSO
Scintillation mechanism	No	No	No	No	No	No
Phosphorescence (afterglow)	Yes	Yes	Yes	Yes	Yes	Yes
Absorption (color centers)	Yes	Yes	Yes	Yes	Yes	Yes
Recover at room temperature	Slow	Slow	No	Yes	Yes	No
Dose-rate dependence	No	No	No	Yes	Yes	No
Thermally annealing	No	No	Yes	Yes	Yes	Yes
Optical bleaching	No	No	Yes	Yes	Yes	Yes

very low, the color-center density would increase continuously under irradiations until all defect traps are fully filled. In this case, the corresponding radiation damage effect is not dose-rate dependent.

Color centers may also be annihilated thermally by heating the crystal to a high temperature through a process called thermal annealing, or optically by injecting light of various wavelengths to the crystal through a process called optical bleaching (Ma and Zhu 1993, 1995). The recovery process, either spontaneous or manual through thermal annealing or optical bleaching,

reduces the color-center density or the radiation-induced absorption. At the same time, it also introduces an additional instability for the crystal's light output because of the variation of the crystal's transparency. In this case, a precision monitoring system is mandatory to follow the variations of the crystal's transparency.

The radiation damage caused by neutrons and charged hadrons may differ from that caused by γ rays. Studies (Huhtinen et al. 2005, 2006, 2008) on proton-induced radiation damages in PWO crystals, for example, show a very slow (or no) recovery at room temperature, contrary to the radiation damage caused by γ rays. This leads to a cumulative damage in PWO with no dose-rate dependence for hadrons.

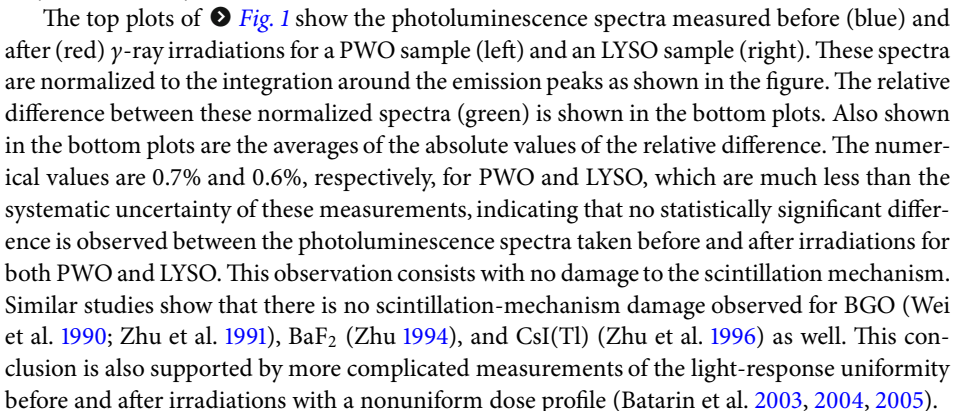
The radiation damage level is also different at different temperatures for crystals with dose-rate-dependent damage since the spontaneous recovery speed is temperature dependent. PWO crystals used at low temperature, for example, suffer more damage than that at high temperature (Semenov et al. 2007, 2008, 2009).

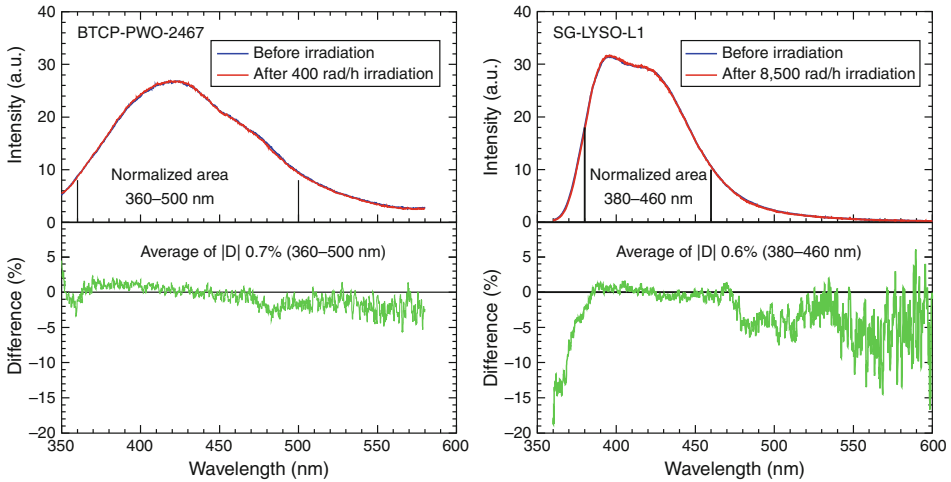
Commercially available mass-produced crystals usually do not meet the quality required for high energy physics detectors. The quality of mass-produced crystals, however, may be improved by removing harmful impurities and defects in the crystal.

The rest of this chapter discusses γ -ray-induced radiation damage phenomena in scintillating crystals, the origin of the radiation damage in halides and oxides, as well as the improvement of crystal quality through systematic R&D. All data presented in this chapter are measured for full-size crystals adequate for calorimeter construction, which is typically 18–25 X_0 long. Since both the radiation-induced phosphorescence and absorption are a bulk effect, it is important that only the full-size crystals are used in such studies.

2 Scintillation-Mechanism Damage

Experimental facts show that the crystal's scintillation mechanism is not damaged. This is observed for irradiations of γ rays, neutrons, as well as charged hadrons (Batarin et al. 2003; Huhtinen et al. 2005, 2006, 2008; Batarin et al. 2004, 2005). A common approach is to compare the shape of the emission spectra measured before and after irradiations. Direct comparison of the overall intensity of the emission spectra suffers from a large systematic uncertainty caused by the sample position and orientation, the surface quality, and the internal absorption which may be induced by the radiation.

The top plots of  Fig. 1 show the photoluminescence spectra measured before (blue) and after (red) γ -ray irradiations for a PWO sample (left) and an LYSO sample (right). These spectra are normalized to the integration around the emission peaks as shown in the figure. The relative difference between these normalized spectra (green) is shown in the bottom plots. Also shown in the bottom plots are the averages of the absolute values of the relative difference. The numerical values are 0.7% and 0.6%, respectively, for PWO and LYSO, which are much less than the systematic uncertainty of these measurements, indicating that no statistically significant difference is observed between the photoluminescence spectra taken before and after irradiations for both PWO and LYSO. This observation consists with no damage to the scintillation mechanism. Similar studies show that there is no scintillation-mechanism damage observed for BGO (Wei et al. 1990; Zhu et al. 1991), BaF₂ (Zhu 1994), and CsI(Tl) (Zhu et al. 1996) as well. This conclusion is also supported by more complicated measurements of the light-response uniformity before and after irradiations with a nonuniform dose profile (Batarin et al. 2003, 2004, 2005).



■ Fig. 1

Normalized photoluminescence spectra measured before (*blue*) and after (*red*) γ -ray irradiation and corresponding difference (*green*) are shown as a function of wavelength for a PWO sample (*left*) and an LYSO sample (*right*)

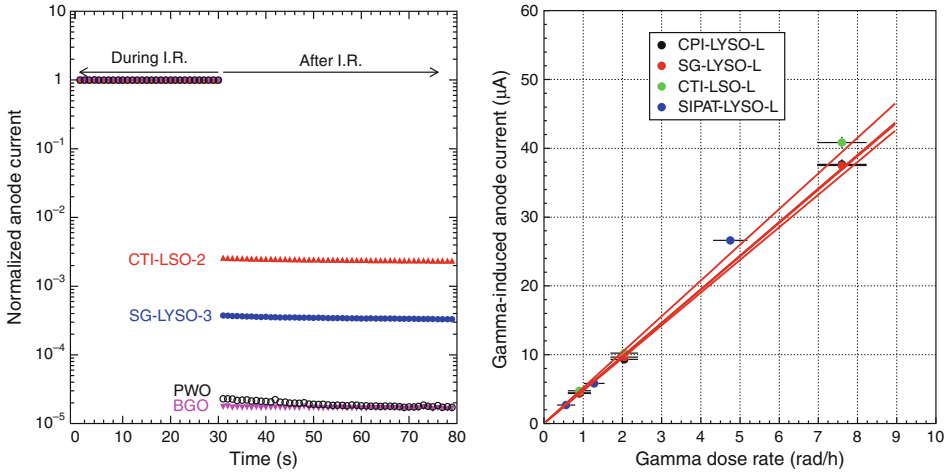
3 Radiation-Induced Phosphorescence and Energy-Equivalent Readout Noise

The radiation-induced phosphorescence can be measured as the residual photocurrent after the radiation is turned off. The left plot of [Fig. 2](#) shows the γ -ray-induced photocurrent, normalized to that during the irradiations, as a function of time during and after the γ -ray irradiations for several crystal samples: PWO, BGO, and LSO/LYSO. All samples are of full size adequate for calorimeter applications. The amplitude of the normalized phosphorescence is at a level of 10^{-5} for BGO and PWO, 3×10^{-4} for LYSO, and 2×10^{-3} for LSO. The LYSO samples are also observed as having a smaller phosphorescence than the LSO sample.

The right plot of [Fig. 2](#) shows γ -ray-induced anode photocurrents as a function of the γ -ray dose rate applied to several LSO and LYSO samples. Consistent slopes are observed for all samples indicating similar light yield for these samples. The slope may be used to calculate the readout noise in the number of electrons for a certain integration gate and be converted to the energy-equivalent readout noise by normalizing to the crystal's light output (Mao et al. 2009a, b). Because of its high light yield (200 times PWO and 5 times BGO) and short decay time (40 ns), the energy-equivalent readout noise in LSO and LYSO is an order of magnitude lower than that in PWO for both γ -ray and neutron irradiations.

4 Radiation-Induced Absorption

The main consequence of radiation damage in scintillation crystals is the radiation-induced absorption or color-center formation. Depending on the type of the defects in the crystal, the color centers may be electrons located in the anion vacancies (F center) and holes located in the



■ Fig. 2

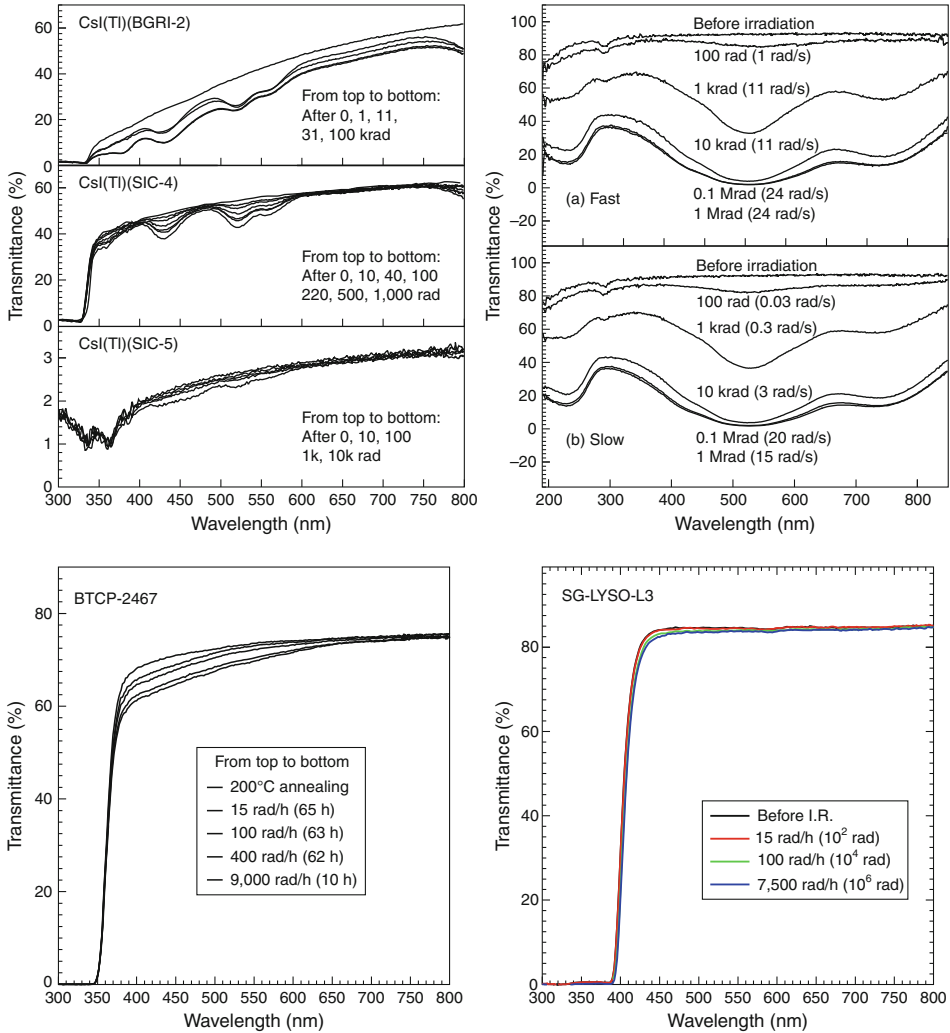
Left: Normalized anode current is shown as a function of time during and after γ -ray irradiations for the BGO, PWO, LSO, and LYSO samples. **Right:** γ -ray-induced anode photocurrent is shown as a function of the dose rate applied to several LSO and LYSO samples

cation vacancies (V center), as well as interstitial anion atoms (H center) or ions (I center), etc. Radiation-induced absorption is observed by comparing the longitudinal optical transmittance spectra measured after and before the irradiations.

► *Figure 3* shows the longitudinal transmittance spectra as a function of wavelength measured before and after several steps of irradiations for four halide crystals: CsI(Tl) (top left) and BaF₂ (top right) and two oxide crystals: PWO (bottom left) and LYSO (bottom right). While the color-center width is narrow in CsI(Tl), it is relatively wide in other crystals. It is interesting to note that the CsI(Tl) sample SIC-5 suffers much less radiation damage than other two CsI(Tl) samples since it was grown with a scavenger in the melt to remove the oxygen contamination, which is an effective approach to improve radiation hardness for the halide crystals as discussed in ► *Sect. 7*. For the BaF₂ sample, we also notice that the fast dose rate (top) is up to a factor of 30 of the slow rate (bottom) while the damage levels of the longitudinal transmittance are identical for the same integrated dose. This is expected since no recovery at the room temperature was observed for BaF₂ as discussed in ► *Sect. 4.3*.

It is also interesting to note that the radiation-induced absorption is much smaller in LSO and LYSO than that in other crystals. ► *Figure 4* shows an expanded view of the longitudinal transmittance spectra measured before and after several steps of γ -ray irradiations for a PWO (left) and an LYSO (right) sample. Also shown in the figure is the corresponding photoluminescence spectra (blue) and the numerical values of the photoluminescence-weighted longitudinal transmittance (EWLT), which is defined as:

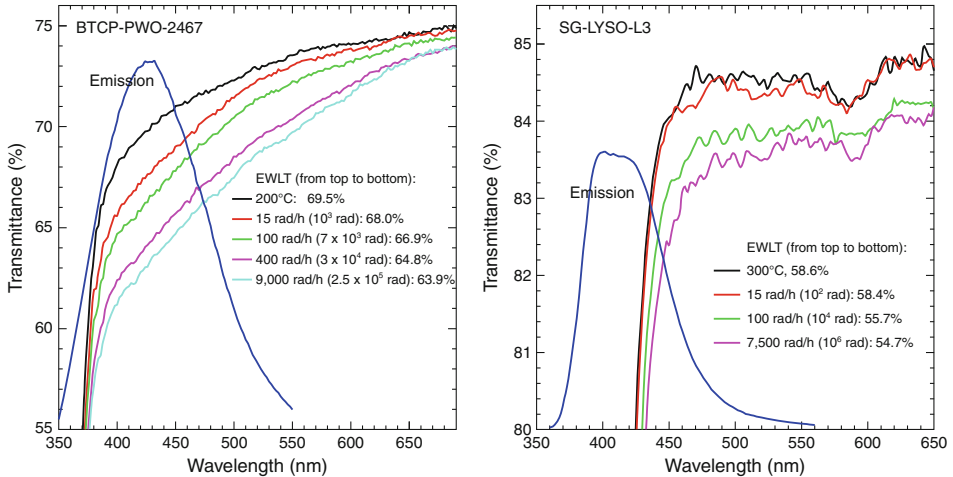
$$\text{EWLT} = \frac{\int LT(\lambda) Em(\lambda) d\lambda}{\int Em(\lambda) d\lambda}. \quad (1)$$



■ Fig. 3

The longitudinal transmittance spectra measured before and after several steps of the irradiation are shown as a function of wavelength for several Csi(Tl) (*top left*), BaF₂ (*top right*), PWO (*bottom left*), and LYSO (*bottom right*) samples

The EWLTV values represent the crystal's transparency more accurately than the transmittance at the emission peak, which is commonly used in various radiation damage studies. This is particularly true for LSO and LYSO, which have a non-negligible self-absorption since their emission spectra are not entirely within the transparent region of the crystal (Chen et al. 2005, 2007).



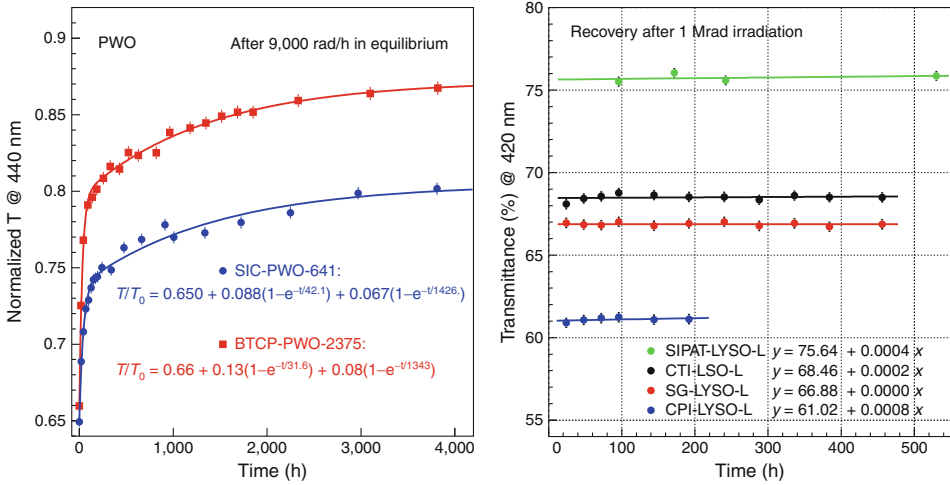
■ Fig. 4

Degradation on EWL for a PWO sample (left) and an LYSO sample (right)

4.1 Recovery of Radiation-Induced Absorption

Depending on the color-center depth, the radiation-induced absorption may recover spontaneously at the room or application temperature. Figure 5 shows the recovery behavior of the longitudinal optical transmittance measured after the γ -ray irradiations up to 4,000 and 500 h, respectively, for two PWO samples at 440 nm (left) and four LSO and LYSO samples at 420 nm (right). Three recovery time constants were determined by using exponential fits for these PWO samples. While the short time constant is at a few tens of hours, the medium time constant is at a few thousand hours, and the third time constant is much longer, which may be considered no recovery for the time scale of these measurements. It is also interesting to note that the LSO and LYSO samples show very slow recovery speed, which is consistent with no recovery. Similarly, the radiation-induced absorption does not recover at the room temperature for BaF_2 (Zhu 1994) and CsI(Tl) (Zhu et al. 1996) as well.

In addition to the spontaneous recovery at the room or application temperature, the radiation damage level may also be reduced by heating crystals to a high temperature (thermal annealing) or injecting light of various wavelengths to the crystal (optical bleaching). The γ -ray-induced absorption can be thermally annealed entirely at 200°C for BaF_2 (Zhu 1994), BGO (Wei et al. 1990; Zhu et al. 1991), and PWO (Zhu et al. 1996, 1998, 1999, 2002, 2004), or 300°C for LSO and LYSO (Chen et al. 2005, 2007). Optical bleaching was also found effective for BaF_2 (Zhu 1994), BGO (Wei et al. 1990; Zhu et al. 1991), and PWO (Zhu et al. 1996, 1998, 1999, 2002, 2004). On the other hand, the γ -ray-induced absorption in CsI(Tl) can neither be annealed thermally or bleached optically (Zhu et al. 1996). Optical bleaching may be used to reduce the color-center density for crystals of poor radiation hardness. It has been extensively studied for BaF_2 (Ma and Zhu 1995) and PWO (Zhu et al. 1996, 1998, 1999, 2002, 2004) in the past and is actively pursued for PWO (Semenov et al. 2007, 2008, 2009). In this case, a precision monitoring is mandatory to follow the variations of the crystal's light output caused by the variations of the crystal's transparency.



■ Fig. 5

The recovery of γ -ray-induced transmittance damage is shown as a function of time after the irradiation for a PWO sample (left) and an LSO/LYSO sample (right)

4.2 Radiation-Induced Color Centers

The longitudinal transmittance data can be used to calculate the light attenuation length of the crystal according to (Ma and Zhu 1993)

$$LAL = \frac{\ell}{\ln \left\{ [T(1 - T_s)^2] / \left[\sqrt{4T_s^4 + T^2(1 - T_s^2)^2} - 2T_s^2 \right] \right\}}, \quad (2)$$

where T is the longitudinal transmittance measured along crystal length ℓ , and T_s is the theoretical transmittance assuming multiple bouncing between two crystal ends and without internal absorption:

$$T_s = (1 - R)^2 + R^2(1 - R)^2 + \dots = (1 - R)/(1 + R), \quad (3)$$

and

$$R = \frac{(n_{\text{crystal}} - n_{\text{air}})^2}{(n_{\text{crystal}} + n_{\text{air}})^2}, \quad (4)$$

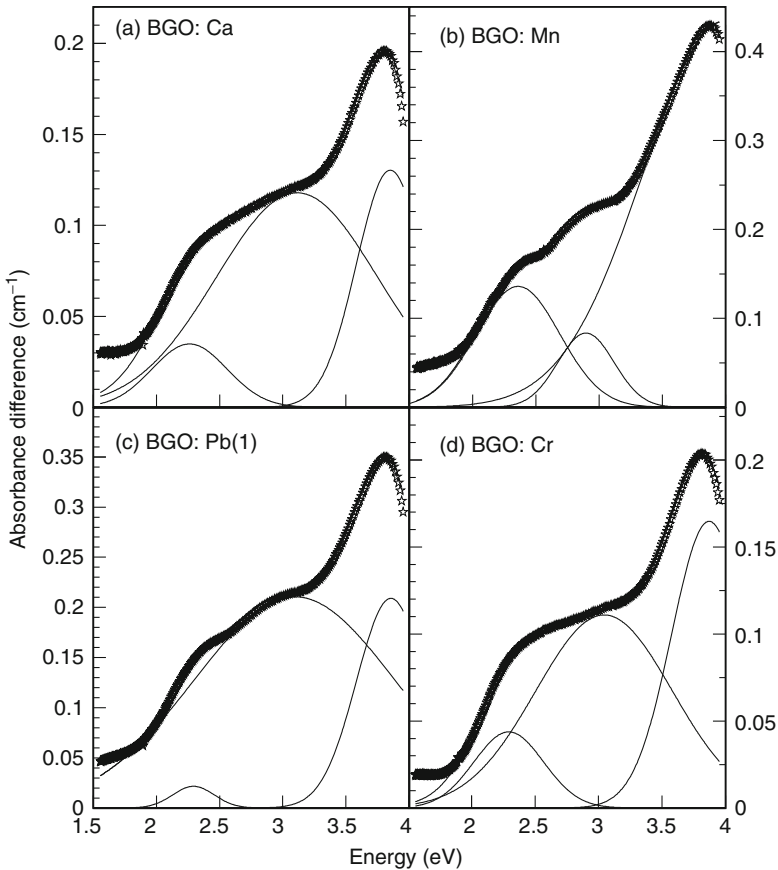
where n_{crystal} and n_{air} are the refractive indices for crystal and air, respectively.

The radiation-induced absorption coefficient, or the color-center density D , can be calculated according to (Ma and Zhu 1993, 1995)

$$D = 1/LAL_{\text{after}} - 1/LAL_{\text{before}}, \quad (5)$$

where LAL_{after} and LAL_{before} are the light attenuation lengths after and before the irradiation.

The radiation-induced absorption-coefficient spectrum can also be presented as a function of the photon energy and be further decomposed to a sum of several color centers with Gaussian energy distributions (Wei et al. 1990; Zhu et al. 1991).



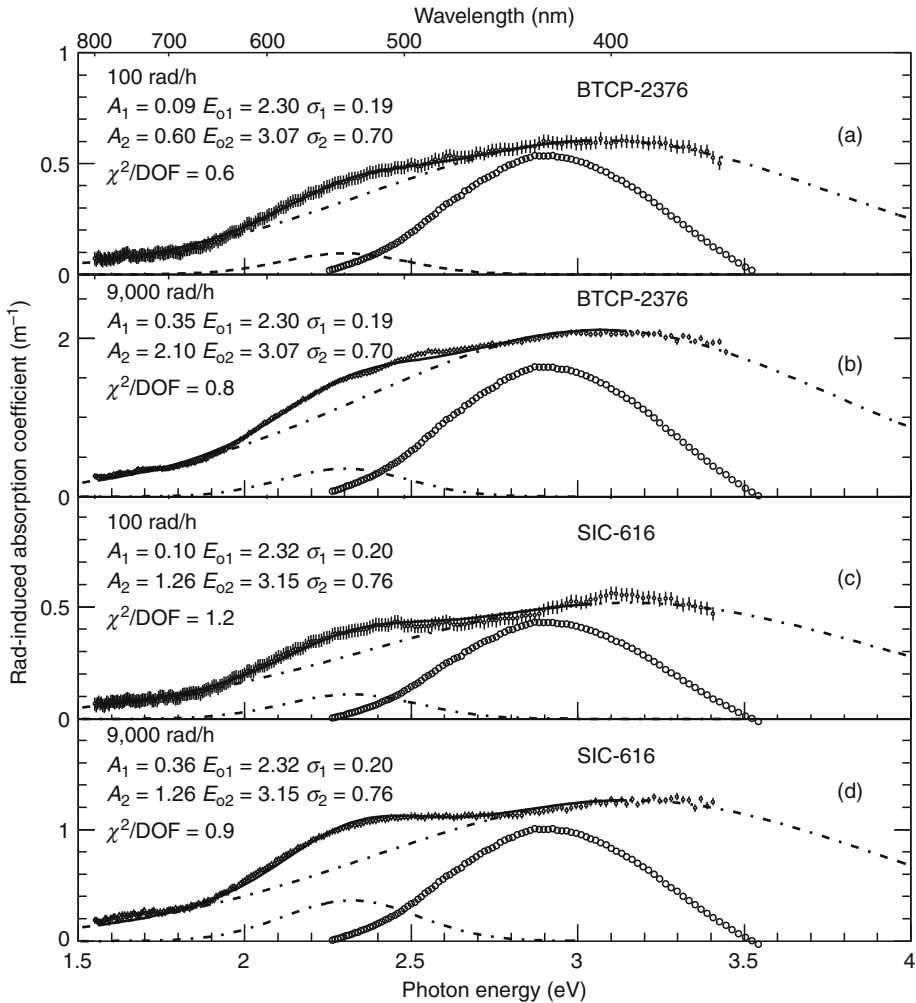
■ Fig. 6

The radiation-induced absorption-coefficient spectra (*lines with stars on top*) are shown as a function of the photon energy for four doped BGO samples. The spectra are decomposed to sums of three color centers (*plain solid lines*)

$$D = \sum_{i=1}^n A_i e^{-\frac{(E-E_i)^2}{2\sigma_i^2}}, \quad (6)$$

where E_i , σ_i , and D_i denote the energy, width, and amplitude of the color center i , and E is the photon energy.

► **Figures 6** and ► **7** show the radiation-induced color-center densities plotted as a function of the photon energy, respectively, for four BGO samples doped with Ca, Mn, Pb, and Cr (left) and two PWO samples in the equilibrium under the γ -rays irradiations with dose rate of 100 rad/h and 9,000 rad/h (right). It is interesting to note that although the overall shapes of these radiation-induced absorption coefficients are rather different, the Gaussian decompositions show the color centers located at the same energy and with the same width. While there



■ Fig. 7

The radiation-induced absorption-coefficient spectra (*data points with error bars*) are shown as a function of the photon energy for two PWO samples in the equilibrium at two different dose rates. The spectra are decomposed to sums of two color centers (*dot-dashed lines*). Also shown in the figure is the emission spectrum of PWO

are three color centers peaked at 2.3, 3.0, and 3.8 eV for all BGO samples, the PWO samples show two color centers peaked at 2.3 and 3.1 eV.

These observations hint that the color centers in these oxide crystals are caused by crystal-structure-related defects, such as oxygen vacancies, not particular impurities. The readers are referred to the corresponding references (Wei et al. 1990; Zhu et al. 1991, 1996, 1998, 1999, 2002, 2004) for more discussions about these color centers.

4.3 Dose-Rate Dependence and Color-Center Kinetics

Because of the balance between two processes – the color-center creation (irradiation) and the color-center annihilation (room-temperature recovery) – the radiation damage may be dose-rate dependent. Assuming that the annihilation speed of the color center i is proportional to a constant a_i and its creation speed is proportional to a constant b_i and the dose rate (R), the differential change of color-center density when both processes coexist can be expressed as (Ma and Zhu 1993, 1995):

$$dD = \sum_{i=1}^n \left\{ -a_i D_i dt + \left(D_i^{\text{all}} - D_i \right) b_i R dt \right\}, \quad (7)$$

where D_i is the density of the color center i in the crystal and the summation goes through all the centers. The solution of \blacktriangleright Eq. 7 is

$$D = \sum_{i=1}^n \left\{ \frac{b_i R D_i^{\text{all}}}{a_i + b_i R} \left[1 - e^{-(a_i + b_i R)t} \right] + D_i^0 e^{-(a_i + b_i R)t} \right\}, \quad (8)$$

where D_i^{all} is the total density of the trap related to the color center i and the D_i^0 is its initial value. The color-center density in the equilibrium (D_{eq}) depends on the dose rate (R):

$$D_{\text{eq}} = \sum_{i=1}^n \frac{b_i R D_i^{\text{all}}}{a_i + b_i R}. \quad (9)$$

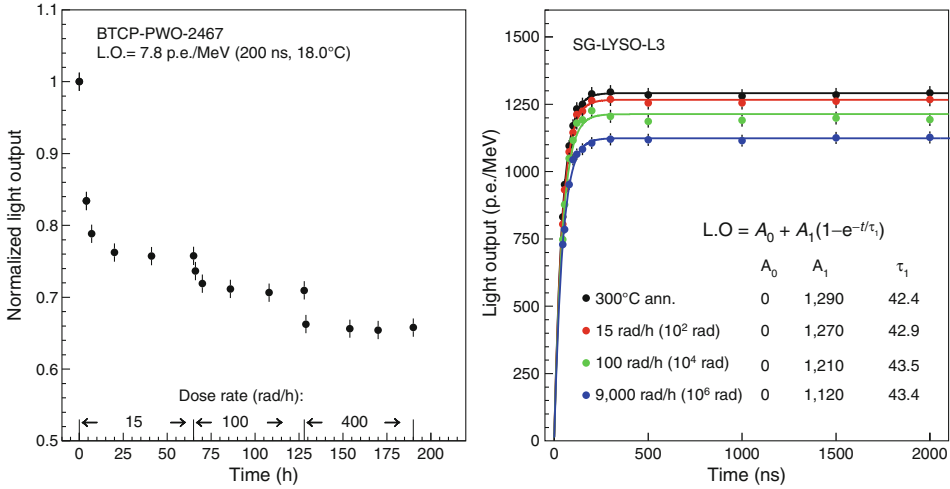
Following this equation, the optical transmittance, and thus the light output, would decrease when crystals are exposed to a radiation with a certain dose rate until they reach an equilibrium. At the equilibrium the speed of the color-center formation (damage) equals to the speed of the color-center annihilation (recovery), so that the color-center density (radiation-induced absorption) does not change unless the dose rate applied changes. More detailed discussions on the behavior of the color centers with bleaching light can be found in Ma and Zhu (1993, 1995).

\blacktriangleright Equation 9 also indicates that the damage level is not dose-rate dependent if the recovery speed (a_i) is small, which is the characteristics of the radiation damage caused by deep color centers. For crystals with no dose-rate dependence, an accelerated irradiation with a high dose rate would reach the same result as a slow irradiation with a low dose rate provided that the total integrated dose is the same. This is clearly shown in the transmittance data of a BaF₂ crystal in the top right plot of \blacktriangleright Fig. 3.

5 Light-Output Degradation

The light output of a crystal scintillator is a convolution of the crystal's emission spectrum, the light propagation inside the crystal, and the quantum efficiency (QE) of the photodetector. All these are wavelength-dependent. Although the crystal emission and photodetector QE are not affected by the radiation, the efficiency of the light propagation is affected by the variations of the light attenuation length and thus the radiation damage.

The left plot of \blacktriangleright Fig. 8 shows the normalized light output as a function of time when the γ rays are applied at a defined dose-rate step by step from 15 rad/h up to 400 rad/h for a PWO sample. The dose-rate dependence of the γ -ray-induced radiation damage in PWO is clearly



■ Fig. 8

Left: The normalized light output is shown as a function of time during several steps of the γ -ray irradiations with the dose rate up to 400 rad/h for a PWO sample. **Right:** The light output is shown as a function of the integration time after several steps of γ -ray irradiations with integrated dose up to 1 Mrad for an LYSO sample

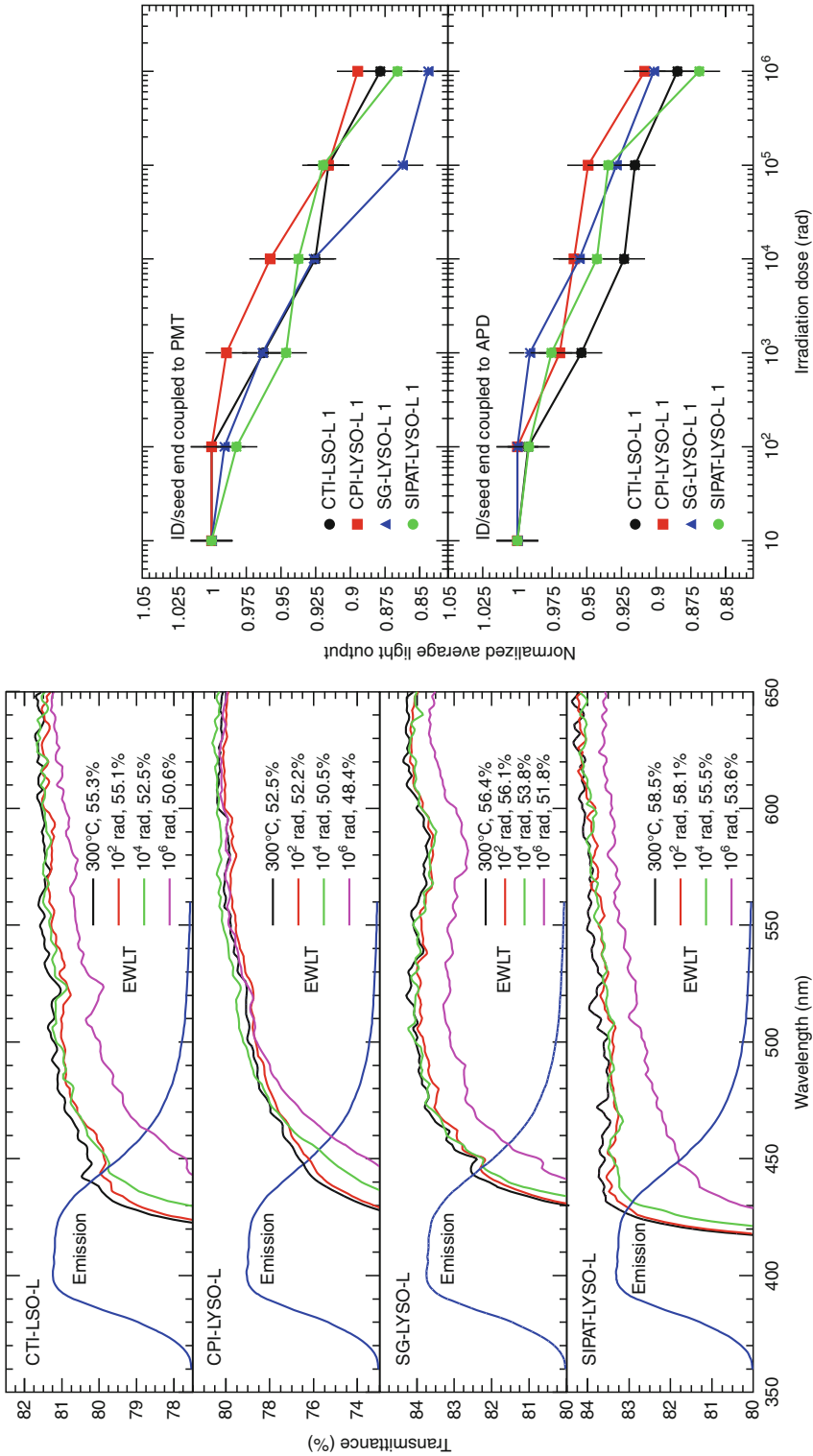
shown. The right plot of [Fig. 8](#) shows the light output as a function of the integration time together with the exponential fits to the scintillation decay time for a LYSO sample after several steps of irradiations with the cumulated dose up to 1 Mrad. It is clear that while the light output degrades the scintillation decay time remains the same, which is consistent with no damage to the scintillation mechanism.

The radiation hardness of LSO and LYSO crystals against γ rays (Mao et al. 2009a), neutrons (Mao et al. 2009b), and charged hadrons (Nessi-Tedaldi et al. 2009) has been found to be excellent. [Figure 9](#) shows the expanded longitudinal transmittance spectra (left) and the normalized average light output (right) for four LSO and LYSO samples. For the light-output measurement the seed/ID end of these samples is coupled to the readout device: XP2254 PMT (top) and two S8664-55 APDs (bottom). All samples tested have a consistent radiation resistance, with the degradations of the EWLT and the light output of approximately 12% for a γ -ray dose of 1 Mrad. Because of these advantages, LYSO crystals are being considered for several future HEP experiments, such as SuperB and the CMS endcap calorimeter upgrade.

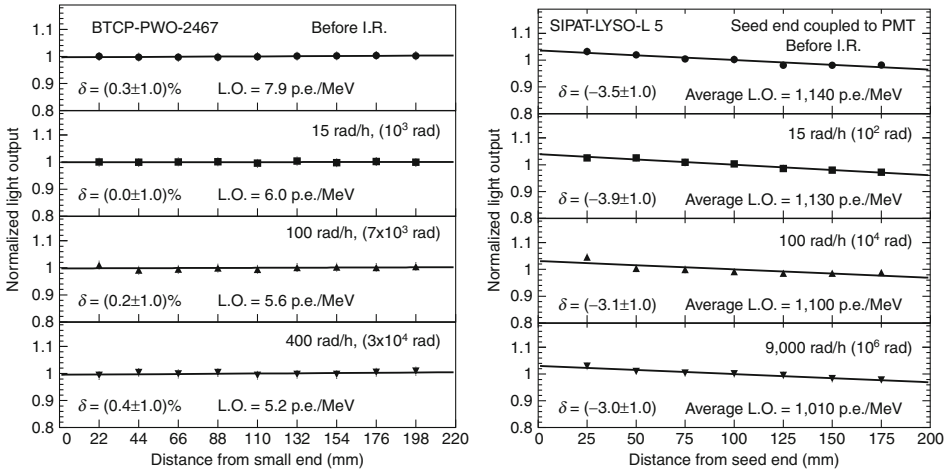
6 Light-Response Uniformity

An adequate light-response uniformity along the crystal length is a key for maintaining the crystal precision at high energies. The light-response uniformity of a long crystal may be parameterized as a linear function

$$\frac{LY}{LY_{\text{mid}}} = 1 + \delta(x/x_{\text{mid}} - 1), \quad (10)$$



■ Fig. 9 The longitudinal transmittance spectra (left) and the normalized light output (right) are shown as a function of the integrated dose for four long LSO and LYSO samples



■ Fig. 10

The light-response uniformity as a function of the distance to the small end and the end coupled to the PMT for a PWO sample (left) and an LYSO sample (right), respectively, after several steps of γ -ray irradiations

where (LY_{mid}) represents the light output measured at the middle point of the crystal, δ represents the deviation from the flat response, and x is the distance from one end of the crystal.

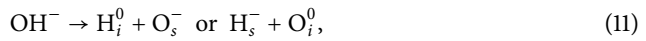
► Figure 10 shows the light-response uniformity after several steps of the γ -ray irradiations for a PWO sample (left) and an LYSO sample (right). The γ -ray irradiations were carried out step by step under a fixed dose rate in each step for the PWO sample. It is clear that the shape of the light-response uniformity was not changed for both crystals, indicating that the energy resolution is not compromised by the γ -ray irradiations. This is due to the fact that the degraded light attenuation length is long enough to maintain the light-response uniformity as predicted by a ray-tracing simulation for the light propagation inside the crystal (Zhu 1998).

7 Damage Mechanism in Alkali Halide Crystals and CsI(Tl) Development

Material analysis is crucial for identifying the radiation damage mechanism. The Glow Discharge Mass Spectroscopy (GDMS) analysis was used to search for correlations between the trace impurities in the CsI(Tl) crystals and their radiation hardness. Samples were taken 3–5 mm below the surface of the crystal to avoid surface contamination. A survey of 76 elements, including all of the lanthanides, indicates that there are no obvious correlations between the detected trace impurities and the crystal's susceptibility to the radiation damage. This indicates an important role of the oxygen contamination which cannot be determined by the GDMS analysis.

Oxygen contamination is known to cause radiation damage in the alkali halide scintillators. In BaF₂ (Zhu 1994), for example, hydroxyl (OH⁻) may be introduced into crystal through a

hydrolysis process and later decomposed to interstitial and substitutional centers by radiation through a radiolysis process. Equation 11 shows a scenario of this process:



where the subscript i and s refer to the interstitial and substitutional centers, respectively. Both the O_s^- center and the U center (H_s^-) were identified (Zhu 1994).

Following the BaF_2 experience, significant improvement of the radiation hardness was achieved for CsI(Tl) crystals by using a scavenger to remove oxygen contamination (Zhu et al. 1996). Figure 11 (left) shows the normalized light output as a function of the integrated dose for several CsI(Tl) samples, and compared to the *BaBar* radiation-hardness specification (solid line) (Zhu 1998). While the late samples SIC-5, 6, 7, and 8 satisfy the *BaBar* specification, early samples SIC-2 and 4 do not.

The improvement of the CsI(Tl) quality was achieved following an understanding that the radiation damage in the halide crystals is caused by the oxygen or hydroxyl contamination. Various material analyses were carried out to quantitatively identify the oxygen contamination in the CsI(Tl) samples. Gas Fusion (LECO) was found not sensitive enough to identify the oxygen contamination in CsI(Tl) samples. The identification of oxygen contamination was achieved by using the Secondary Ionization Mass Spectroscopy (SIMS) analysis. A Cs ion beam of 6 keV and 50 nA was used to bombard the CsI(Tl) sample. All samples were freshly cleaved prior to being loaded into the UHV chamber. An area of $0.15 \times 0.15 \text{ mm}^2$ on the cleaved surface was analyzed. To further avoid the surface contamination, the starting point of the analysis is at about 10 μm deep inside the freshly cleaved surface. The right plot of Fig. 11 shows the depth profile of the oxygen contamination for two radiation-soft samples (SIC-T1 and SIC-2) and two rad-hard samples (SIC-T3 and Khar'kov)

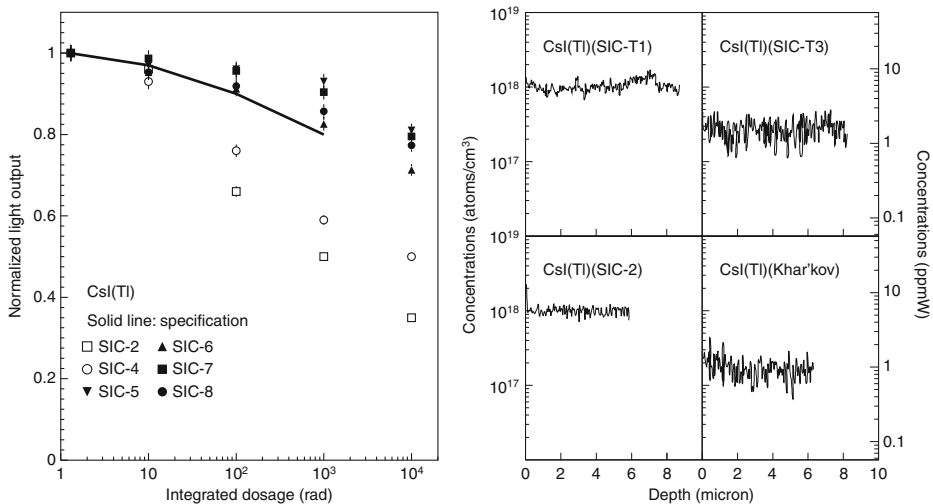


Fig. 11

Left: The progress of the CsI(Tl) radiation hardness is shown for CsI(Tl) samples together with the *BaBar* radiation-hardness specification. Right: The depth profile of the oxygen contamination is shown for two rad-soft CsI(Tl) samples (SIC-T1 and SIC-2) and two rad-hard samples (SIC-T3 and Khar'kov)

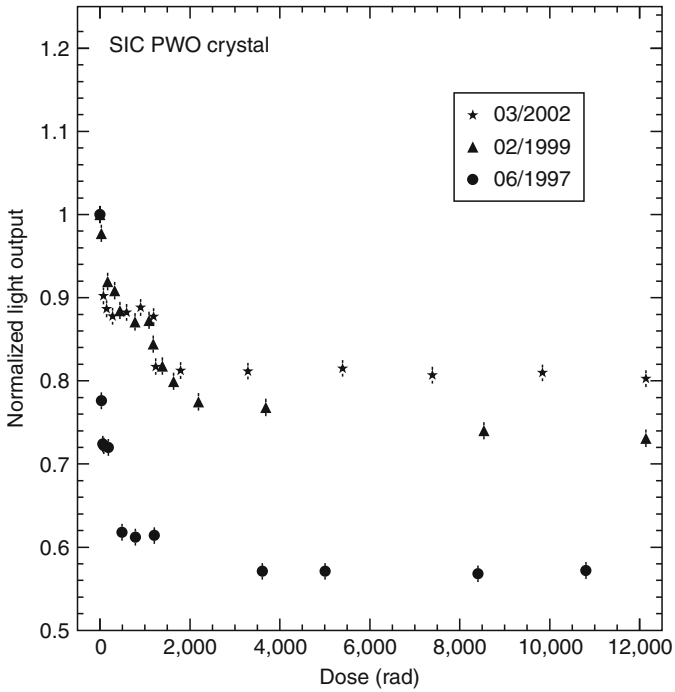
and two radiation-hard samples (SIC-T3 and Khar'kov). Crystals with poor radiation resistance have oxygen contamination of 10^{18} atoms/cm³ or 5.7 PPMW, which is five times higher than the background count (2×10^{17} atoms/cm³, or 1.4 PPMW).

8 Damage Mechanism in Oxide Crystals and PWO Development

Similarly, GDMS analysis was carried out for BGO and PWO crystals, and was found to have no particular correlation with the crystal's radiation hardness. This hints an important role of the structure-related defects in the crystal which cannot be determined by the GDMS analysis. Crystal structure defects, such as oxygen vacancies, are known to cause radiation damage in oxide scintillators. In BGO, for example, three common radiation-induced absorption bands at 2.3, 3.0, and 3.8 eV were found in a series of 24 doped samples (Wei et al. 1990; Zhu et al. 1991) as shown in [Fig. 6](#). Observations in the PWO crystals are similar with two color centers peaked at 2.3 and 3.1 eV as shown in [Fig. 7](#). Following these observations, effort was made to reduce the oxygen vacancies in PWO crystals. An oxygen compensation approach, which was carried out by a post-growth thermal annealing in an oxygen-rich atmosphere, was found effective in improving PWO's radiation hardness for samples up to 10 cm long (Zhu et al. 1996, 1998, 1999, 2002, 2004). This approach, however, is less effective for longer (25 cm) crystals which show a variation of the oxygen vacancies along the crystal. In practice, yttrium doping, which provides a local charge balance for oxygen vacancies and so prevents the color-center formation, was found effective for PWO (Zhu et al. 1996, 1998, 1999, 2002, 2004). [Figure 12](#) shows the normalized light output as a function of time for three PWO samples under the γ -ray irradiations with a dose rate of 15 rad/h. PWO samples, produced in late 2002 with yttrium doping, are much more radiation hard than the early samples.

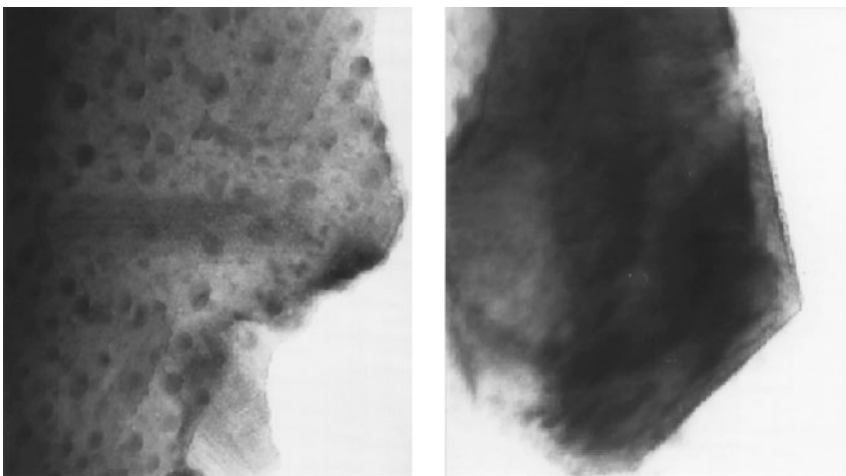
This improvement of PWO quality was achieved following an understanding that the radiation damage in the oxide crystals is caused by the oxygen vacancies. Various material analyses were carried out to quantitatively identify the stoichiometry deviation and the oxygen vacancies in the PWO samples. Particle-Induced X-ray Emission (PIXE) and quantitative wavelength-dispersive Electron Micro-Probe Analysis (EMPA) were tried. PWO crystals with poor radiation hardness were found as having a non-stoichiometric W/Pb ratio. Both PIXE and EMPA, however, does not provide the oxygen analysis. X-ray Photoelectron Spectroscopy (XPS) was found to be very difficult because of the systematic uncertainty in oxygen analysis. Electron Paramagnetic (or Spin) Resonance (EPR or ESR) and Electron-Nuclear Double Resonance (ENDOR) were tried to find unpaired electrons, but were also found to be difficult to reach a quantitative conclusion.

The identification of the oxygen vacancies is achieved by using the Transmission Electron Microscopy (TEM) coupled to Energy Dispersion Spectrometry (EDS) with a localized stoichiometry analysis. A TOPCON-002B Scope was first used at 200 kV and 10 μ A. The PWO samples were made to powders of an average grain size of a few μ m and then placed on a sustaining membrane. With a spatial resolution of 2 \AA , the lattice structure of the PWO samples was clearly visible. [Figure 13](#) (left) shows a TEM picture taken for a sample with poor radiation hardness. Black spots of a diameter of 5–10 nm were clearly seen in the picture. On the other hand, the samples with good radiation hardness show a stable TEM picture with no black spots, as shown in [Fig. 13](#) (right). By employing TEM/EDS, a localized stoichiometry analysis



■ Fig. 12

The progress of PWO radiation hardness is shown for PWO samples from SIC



■ Fig. 13

TEM pictures of a PWO crystal of poor radiation hardness (*left*), showing clearly the black spots of \varnothing 5–10 nm related to oxygen vacancies, as compared to that of a good one (*right*)

■ **Table 3**

Atomic fraction (%) of O, W, and Pb in PWO samples measured by TEM/EDS (Yin et al. 1997)

As-grown sample				
Element	Black Spot	Peripheral	Matrix ₁	Matrix ₂
O	1.5	15.8	60.8	63.2
W	50.8	44.3	19.6	18.4
Pb	47.7	39.9	19.6	18.4
The same sample after oxygen compensation				
Element	Point ₁	Point ₂	Point ₃	Point ₄
O	59.0	66.4	57.4	66.7
W	21.0	16.5	21.3	16.8
Pb	20.0	17.1	21.3	16.5

was carried out. The system is a JEOL JEM-2010 scope and a Link ISIS EDS. The spatial resolution of this system allows a localized stoichiometry analysis in a region of a diameter of 0.5 nm. Black lack spots were observed in an as-grown sample. Localized stoichiometry analysis was carried out for points inside and surrounding the black spots, as well as points far away from the black spots. The uncertainty of the analysis is about 15%. The resultant atomic fractions (%) at these areas are listed in ● [Table 3](#) (Yin et al. 1997).

A clear deviation from the atomic stoichiometry of O:W:Pb = 66:17:17 was observed for samples taken inside these black spots, pointing to a severe deficit of the oxygen component. In the peripheral area, the oxygen deficit was less, but still significant. There was no oxygen deficit observed in the area far away from the black spots. As a comparison, the same sample after a thermal annealing in an oxygen-rich atmosphere was reanalyzed. No black spot was found. The result of the analysis is also listed in ● [Table 3](#). In all randomly selected points no stoichiometric deviation was observed. This analysis thus clearly identified oxygen vacancies in PWO samples of poor radiation hardness.

9 Conclusion

Crystal scintillators suffer from radiation damage with possible effects including: (1) the scintillation-mechanism damage, (2) the radiation-induced phosphorescence, and (3) the radiation-induced absorption. No experimental evidence has been observed for the scintillation-mechanism damage in any crystals studied so far. All crystals show the radiation-induced phosphorescence and absorption. The radiation-induced phosphorescence increases the dark current of the photodetector, and thus the readout noise. The energy-equivalent noise is low for crystals with high light yield. The predominant radiation damage effect in the crystal scintillators is the radiation-induced absorption, or color-center formation. The radiation-induced absorption may recover spontaneously at the application temperature and leads to dose-rate dependence. Thermal annealing and optical bleaching are also found to be effective for shallow color centers, but not for all crystal scintillators.

The radiation damage in the alkali halide crystals is understood to be caused by the oxygen and/or hydroxyl contamination as shown by the SIMS analysis. By using a scavenger to remove the oxygen contamination, the radiation hardness of the mass-produced CsI(Tl)

crystals is improved. The radiation damage in the oxide crystals is understood to be caused by the stoichiometry-related defects, for example oxygen vacancies, as shown by the localized stoichiometry analysis with TEM/EDS. By using yttrium doping, the radiation hardness of the mass-produced PWO crystals is improved.

Acknowledgments

Measurements at Caltech were carried out by Drs. J.M. Chen, Q. Deng, H Wu, D.A. Ma, R.H. Mao, X.D. Qu and L.Y. Zhang. This work was supported in part by the US Department of Energy under grant DE-FG03-92-ER-40701 and the US National Science Foundation Award PHY-0612805.

References

- Batarin VA, Butkler J, Chen TY, Davidenko AM, Derevschikov AA, Goncharenko YM et al (2003) Study of radiation damage in lead tungstate crystals using intense high-energy beams. *Nucl Instr Meth A* 512:488–505, A530:286–292 (2004) and A540:131–139 (2005)
- Chen JM, Mao RH, Zhang LY, Zhu R-Y (2005) Large size LYSO crystals for future high energy physics experiments. *IEEE Trans Nucl Sci* 52:2133–2140 (2005) and *IEEE Trans Nucl Sci* 54:718–724 (2007)
- Cooke DW, McClellan KJ, Bennett BL, Roper JM, Whittaker MT, Muenchausen RE (2000) Crystal growth and optical characterization of cerium-doped $Lu_{1.8}Y_{0.2}SiO_5$. *J Appl Phys* 88:7360–7362
- Gratta G, Newman H, Zhu R-Y (1994) Crystal calorimeters in particle physics. *Annu Rev Nucl Part Sci* 44:453–500
- Huhtinen M, Lecomte P, Luckey D, Nessi-Tedaldi F, Pauss F (2005) High-energy proton induced damage in $PbWO_4$ calorimeter crystals. *Nucl Instr Meth A* 545:63, A564:164 (2006) and A587:266 (2008)
- Kimble T, Chou M, Chai BHT (2002) Scintillation properties of LYSO crystals. In: *IEEE NSS Conference Record*, Norfolk, pp 1434–1437
- Ma DA, Zhu R-Y (1993a) Light attenuation length of barium fluoride crystals. *Nucl Instr Meth A* 333:422–424
- Ma DA, Zhu R-Y (1993) On optical bleaching of barium fluoride crystals. *Nucl Instr Meth A* 332: 113–120 and *Nucl Instr Meth A* 356:309–318 (1995)
- Mao RH, Zhang LY, Zhu R-Y (2008) Optical and scintillation properties of inorganic scintillators in high energy physics. *IEEE Trans Nucl Sci* NS-55:2425–2431
- Mao RH, Zhang LY, Zhu R-Y (2009a) Gamma ray induced radiation damage in PWO and LSO/LYSO crystals. Paper N32-5 in *IEEE NSS 2009 Conference Record*
- Mao RH, Zhang LY, Zhu R-Y (2009b) Effect of neutron irradiations in various crystal samples of large size for future crystal calorimeter. Paper N32-4 in *IEEE NSS 2009 Conference Record*
- Melcher C, Schweitzer J (1992) Cerium-doped Lutetium oxyorthosilicate: a fast efficient new scintillator. *IEEE Trans Nucl Sci* NS-39:502–505
- Nessi-Tedaldi F, Dissertori G, Lecomte P, Luckey D, Pauss F (2009) Studies of Cerium fluoride, LYSO and lead tungstate crystals exposed to high hadron fluences. Paper N32-3 in *IEEE NSS 2009 Conference Record*
- Semenov PA, Uzunia AV, Davidenko AM, Derevschikov AA, Goncharenko YM, Kachanov VA et al (2007) First study of radiation hardness of lead tungstate crystals at low temperature. *Nucl Instr Meth A* 562:575–580, *IEEE Trans Nucl Sci* NS-55:1283–1288 (2008) and Paper N32-2 in *IEEE NSS 2009 Conference Record* (2009)
- Wei ZY, Zhu RY, Newman H, Yin ZW (1990) Radiation resistance and fluorescence of Europium doped BGO crystals. *Nucl Instr Meth A* 297:163–168
- Yin ZW, Li PJ, Feng JW (1997) TEM study on lead tungstate crystals. In: Zhiwen Yin et al (eds) *Proceedings of SCINT97 International Conference*. CAS, Shanghai Branch, pp 191–194
- Zhu RY (1994) On quality requirements to the barium fluoride crystals. *Nucl Instr Meth A* 340:442–457
- Zhu RY (1997) Precision crystal calorimetry in future high energy colliders. In: *IEEE NSS1996 Conference Record*, published in *IEEE Trans Nucl Sci* NS-44:468–476

- Zhu R-Y (1998) Radiation damage in scintillating crystals. *Nucl Instr Meth A*413:297–311 and references therein
- Zhu RY, Stone H, Newman H, Zhou TQ, Tan HR, He CF (1991) A study on radiation damage in doped BGO crystals. *Nucl Instr Meth A*302:69–75
- Zhu RY, Ma DA, Wu H (1996) CsI(Tl) radiation damage and quality improvement. In: Antonelli A et al (eds) *Proceedings of the 6th International Conference on Calorimetry in High Energy Physics*. Frascati Physics Series, Bologna, Italy, 589–598
- Zhu RY, Ma DA, Newman HB, Woody CL, Kierstead JA, Stoll SP, Levy PW (1996) A study on the properties of lead tungstate crystals. *Nucl Instr Meth A*376:319–334 (1996), *IEEE Trans Nucl Sci* 45:688–691 (1998), *Nucl Instr Meth A*438:415–420 (1999), *Nucl Instr Meth A*480:470–487 (2002) and *IEEE Trans Nucl Sci* 51:1777–1783 (2004)

Further Reading

- Claeys C, Simoen E (2002) *Radiation effects in advanced semiconductor materials and devices*. Springer, Berlin
- Gruppen C, Shwartz B (2008) *Particle detectors*. Cambridge University Press, Cambridge
- Holmes-Siedle A, Adams L (2002) *Handbook of radiation effects*. Oxford University Press, Oxford
- Iniewski K (2010) *Radiation effects in semiconductors*. CRC Press, Boca Raton
- Knoll G (2000) *Radiation detection and measurement*, 3rd edn. Wiley, New York
- Lecoq P, Annekov A, Gektin A, Korzhik M, Pedrini C (2005) *Inorganic scintillators for detector systems*. Springer-Verlag, Berlin, Heidelberg

